BIOCHEMISTRY
including biophysical chemistry & molecular biology
Article

Biochemistry **2010,** *49,* 2443–2453 2443
DOI: 10.1021/bi902130j

Direct Interaction of the Mouse Cytomegalovirus m152/gp40 Immunoevasin with RAE-1 Isoforms†

Li Zhi,‡ Janet Mans,‡,∥,@ Michael J. Paskow,‡ Patrick H. Brown,§ Peter Schuck,§ Stipan Jonjić,⊥ Kannan Natarajan,‡ and David H. Margulies*,‡

‡*Molecular Biology Section, Laboratory of Immunology, National Institute of Allergy and Infectious Diseases, and* §*Dynamics of Macromolecular Assembly, Laboratory of Bioengineering and Physical Science, National Institute of Biomedical Imaging and Bioengineering, National Institutes of Health, Bethesda, Maryland 20892,* ∥*University of the Witwatersrand, Johannesburg 2050, South Africa, and* ⊥*Department of Histology and Embryology, Faculty of Medicine, University of Rijeka, 51000 Rijeka, Croatia.* @*Current address: Department of Medical Virology, University of Pretoria, Pretoria 0001, South Africa.*

Received December 11, 2009; Revised Manuscript Received February 18, 2010

ABSTRACT: Cytomegaloviruses (CMVs) are ubiquitous species-specific viruses that establish acute, persistent, and latent infections. Both human and mouse CMVs encode proteins that inhibit the activation of natural killer (NK) cells by downregulating cellular ligands for the NK cell activating receptor, NKG2D. The MCMV glycoprotein m152/gp40 downregulates the surface expression of RAE-1 to prevent NK cell control in vivo. So far, it is unclear if there is a direct interaction between m152 and RAE-1 and, if so, if m152 interacts differentially with the five identified RAE-1 isoforms, which are expressed as two groups in MCMV-susceptible or -resistant mouse strains. To address these questions, we expressed and purified the extracellular domains of RAE-1 and m152 and performed size exclusion chromatography binding assays as well as analytical ultracentrifugation and isothermal titration calorimetry to characterize these interactions quantitatively. We further evaluated the role of full-length and naturally glycosylated m152 and RAE-1 in cotransfected HEK293T cells. Our results confirmed that m152 binds RAE-1 directly, relatively tightly (K_d < 5 μM), and with 1:1 stoichiometry. The binding is quantitatively different depending on particular RAE-1 isoforms, corresponding to the susceptibility to downregulation by m152. A PLWY motif found in RAE-1β, although contributing to its affinity for m152, does not influence the affinity of RAE-1γ or RAE-1δ, suggesting that other differences contribute to the RAE-1−m152 interaction. Molecular modeling of the different RAE-1 isoforms suggests a potential site for the m152 interaction.

Cytomegaloviruses (CMVs), ubiquitous species-specific large DNA viruses, possess a remarkable array of immunomodulatory mechanisms that permit evasion of the host's immune response (*1*, *2*). The immunocompetent host employs both innate and adaptive arms of the immune system, exemplified by the natural killer (NK)[1] cell and $CD8^+$ T cell responses, respectively, to control both acute infection and reactivation of latent infection (*1*, *3*, *4*). Accordingly, both mouse CMV (MCMV) and human CMV (HCMV) employ genes to prevent recognition of infected cells by NK and $CD8^+$ T cells (*5*−*7*). NK cells effectively kill CMV-infected targets via NK activating receptors, among which NKG2D is one of the most potent and best studied. Ligands for NKG2D include, in mice, three groups of stress-induced MHC-I-like cell surface molecules known as MULT-1, RAE-1, and H60 (*8*) and, in humans, the MHC class I-related chains A and B (MICA and MICB) and a family of UL16 binding and retinoic acid early transcript 1 proteins (ULBP1-ULBP4, RAET1E, and RAET1G) (*9*). NKG2D is found on a variety of immune effector cells, including NK cells, antigen-experienced $CD8^+$ T cells, $\gamma\delta$ T cells, and some activated $CD4^+$ T cells (*10*−*12*). In contrast with the NK cell response, the adaptive cytolytic T cell response to CMV infection is dependent on classical T cell receptor (TCR)-mediated recognition of viral peptides bound to host MHC-I molecules (*5*), but recent evidence indicates that NKG2D may also function as a coreceptor for T cell recognition (*13*). As part of the ongoing coevolution of virus and host, the CMVs have developed mechanisms for preventing the immune response. Two sets of MCMV genes contribute to viral immunoevasion: those that regulate the expression and recognition of NKG2D ligands and those that modulate recognition by $CD8^+$ T cells. The former include MCMV genes *m145*, *m152*, and *m155* that functionally impair the expression of MULT-1, RAE-1, and H60, respectively [*m145* and *m155* work cooperatively with *m138*, as well (*14*, *15*)]. The latter set of MCMV genes includes *m04* and *m06* as well as *m152* which perform similar functions with respect to the classical MHC-I antigen presentation pathway (*16*−*18*).

Among the NKG2D ligands targeted by MCMV, of particular interest are the five murine RAE-1 isoforms (α, β, γ, δ, and ε) that are more than 90% identical in protein sequence, are expressed as glycophosphatidylinositol (GPI)-linked proteins, and are widely expressed in embryonic and tumor cells but not in adult tissues (*19*, *20*). Of the viral immunoevasins, the m152 glycoprotein

†This work was supported by the Intramural Research Program of the National Institute of Allergy and Infectious Diseases.

*To whom correspondence should be addressed: Bldg. 10, Room 11N311, NIAID/NIH, 10 Center Dr., Bethesda, MD 20892-1892. Telephone: (301) 496-6429. Fax: (520) 626-3644. E-mail: dhm@nih.gov.

[1]Abbreviations: AUC, analytical ultracentrifugation; ITC, isothermal titration calorimetry; NK, natural killer; PAGE, polyacrylamide gel electrophoresis; s_w, weight average coefficient; s_{fast}, reaction boundary coefficient; SE, sedimentation equilibrium; SV, sedimentation velocity; SEC, size exclusion chromatography.

Published on Web 02/18/2010

(also known as gp40) is remarkable because it counters both the NK cell and $CD8^+$ T cell recognition pathways (*17*, *21*−*23*), the first by lowering the level of expression of RAE-1, leading to a decreased level of recognition by NKG2D-bearing NK cells, and the second by downregulation of some host MHC-I molecules, influencing T cell recognition of virus-infected cells (*22*). Despite efforts to understand the biochemical basis of the downregulation of RAE-1 by m152, direct interaction of m152 with RAE-1 has not been demonstrated (*24*). Although early studies based on cDNA transfection suggested that all five RAE-1 isoforms were efficiently downregulated at the cell surface by m152 (*21*), other experiments indicated that RAE-1δ was resistant to the effects of m152-mediated downregulation (*24*). An amino acid sequence motif in RAE-1α, -β, and -γ (PLWY) was shown to contribute to differences in the effect of m152 on the different RAE-1 isoforms (*24*).

To elucidate the biochemical basis of the proposed "cis" interaction of m152 with different RAE-1 isoforms, we have engineered RAE-1 and representative mutants for bacterial expression and report here studies, both qualitative and quantitative, of the binding of recombinant m152 with this panel of RAE-1 molecules. Analysis by size exclusion chromatography (SEC) and analytical ultracentrifugation (AUC) reveals direct interaction of m152 with several isoforms of RAE-1, exposing quantitative differences. These studies explore the contribution of the PLWY motif of RAE-1 and suggest a competitive relationship between the m152 and NKG2D binding sites on RAE-1.

EXPERIMENTAL PROCEDURES

Plasmids. cDNA encoding RAE-1β was amplified by PCR using the sense primer (5′ATTCATGTCGACATGGCCAAGGCAGCAGTGAC) and antisense primer (5′GACACGGTCGACTCACATCGCAAATGCAAATGC) from total RNA isolated from NIH3T3 cells (ATCC CRL-1658). RAE-1γ and -δ cDNAs were synthesized (Ezbiolab) and cloned into the SalI restriction site of the pB45-Neo plasmid (*24*). Deletion of the PLWY motif of RAE-1β and -γ was conducted with the Qiagen XL-II mutagenesis kit according to the manufacturer's instructions using oligonucleotides 5′GATCCTACCCCAGCAGATGAAGCGAAGTGCTTCGTG for RAE-1β and 5′GCTCCTACCCCAGCAGATGAAGCGAAGTGCTTAGTG for RAE-1γ. Insertion of PLWY into RAE-1δ was accomplished by gene synthesis (Ezbiolab). pIRES-hr-GFP-II mammalian expression vectors (Stratagene) encoding N-terminally FLAG-tagged versions of m152 and m153 were generated as described previously (*25*).

The portions of the cDNA encoding the ectodomains of m152 (residues 1−310) and m153 (residues 1−314) were cloned into the pMT-Bip-V5-His insect expression vector (Invitrogen) as described previously (*25*) for inducible, secreted expression of proteins in *Drosophila* S2 cells. The portion of the cDNA encoding the ectodomain of RAE-1 proteins [residues 28−205 of RAE-1β or -γ and residues 28−201 of RAE-1δ (see Figure 4)] was cloned into pET21b (Novagen) between NdeI and HindIII restriction sites for expression as inclusion bodies in *Escherichia coli*. [The numbering convention for RAE-1 isoforms is based on the initiation methionine of the signal peptide being amino acid 1 (see Figure 4). Numbering for the X-ray structure of RAE-1 differs by 30 (*26*).] All final constructs were verified by DNA sequencing.

Protein Expression and Purification. Selection, expression, and purification of the ectodomains of m152 and m153 encoded in pMT-Bip-V5-His from *Drosophila* S2 cells (Invitrogen) were described previously (*25*). The supernatant collected from S2 cells after induction with 1 mM Cu^{2+} for 4−6 days was dialyzed against PBS before application to a Ni^{2+}-NTA column (Qiagen) for initial purification, followed by further purification by SEC on a Superdex 75 column (GE Healthcare). (In the literature, the m152 protein is often termed m152/gp40. In this paper, we will refer to the protein as m152 and the encoding gene as *m152*.) The ectodomains of RAE-1 proteins encoded in pET21b (Novagen) were expressed as inclusion bodies in BL21Rosetta (pLysS) cells (Novagen) using the overnight express autoinduction system (Novagen). Inclusion bodies were subsequently solubilized in guanidine and refolded by dilution into an arginine buffer containing a glutathione redox couple (*27*). Refolded proteins were further purified on a Superdex 75 column (GE Healthcare). Protein concentrations were determined by a BCA protein assay with BSA as the standard (Pierce). Similar protocols for *E. coli* expression, in vitro refolding, and purification of RAE-1 isoforms have been used in other laboratories for studies of the interaction of RAE-1 with NKG2D both in binding studies (*28*) and for crystallization and X-ray structure determination (*26*). Following refolding and purification on Superdex 75, all preparations were evaluated for purity by SDS−polyacrylamide gel electrophoresis. All RAE-1 isoforms and mutants were also examined for reactivity with a pan RAE-1 monoclonal antibody (clone 186107, R&D Systems) by surface plasmon resonance, and for reactivity with NKG2D-Fc by an ELISA confirming that these molecules were properly folded. In addition, data from sedimentation velocity (SV) experiments were analyzed to estimate the degree of purity and the frictional ratios (f_r) of each of the preparations used for the AUC studies: $f_r = 1.35$ and >90% pure for m152, $f_r = 1.42$ and >95% pure for RAE-1β, $f_r = 1.43$ and 90% homogeneous for the RAE-1β mutant, $f_r = 1.44$ and 98% homogeneous for RAE-1γ, $f_r = 1.42$ and 99% homogeneous for the RAE-1γ mutant, $f_r = 1.39$ and 99% homogeneous for RAE-1δ, and $f_r = 1.42$ and 99% homogeneous for the RAE-1δ mutant. If a fraction of the molecules were unfolded or aggregated, because of the increased translational friction, the sedimentation coefficients would be distinctly lower and the frictional ratio would be >2.0. Typical frictional ratios for most globular hydrated proteins are between 1.3 and 1.5. Such SV AUC analysis is particularly accurate with regard to the size homogeneity of proteins and serves as a standard for the detection of trace oligomeric impurities (*29*).

Cell Lines and Transfectants. HEK293T (ATCC CRL-11268) cells were cultivated in DMEM supplemented with 10% FCS, 50 μM 2-mercaptoethanol, 1× nonessential amino acids (Bio Whittaker), and 50 μg/mL gentamicin. *Drosophila* S2 cells were cultured in Insect Express medium (Bio Whittaker) supplemented with 50 μg/mL gentamicin. Transient transfection of HEK293T cells was performed using Fugene 6 (Roche) according to the manufacturer's instructions. Briefly, 1.5 μg of pB45-neo encoding RAE-1γ or -δ or their PLWY deletion mutants was mixed with increasing amounts (6, 24, and 96 ng) of either pIRES-hr-GFP III (Invitrogen) alone or pIRES-hr-GFP III encoding m152. The mixture was then added to 5×10^5 HEK293T cells in 2 mL of growth medium along with Fugene 6 and incubated at 37 °C for ~48 h. Cells were then analyzed for surface RAE-1 expression by flow cytometry.

Flow Cytometry. Cells were incubated with PE-conjugated pan anti-RAE-1 mAb 186107 (R&D Systems), isotype control (eBioscience), or Cy3-conjugated anti-FLAG M2 antibody (Sigma). After being washed three times with PBS with 0.5%

BSA and 0.03% NaN_3, samples were examined on a FACSCalibur (Becton Dickinson) and analyzed with FlowJo (Treestar).

Measurement of Binding by Chromatography, Analytical Ultracentrifugation, and Isothermal Titration Calorimetry. Equimolar amounts (~1 nmol, 20 μL of each) of purified RAE-1 and m152 proteins were mixed in TBSE [25 mM Tris-HCl, 150 mM NaCl, and 10 mM EDTA (pH 7.5)] and incubated on ice for 30 min before being loaded on a Shodex PROTEIN KW-803 HPLC gel filtration chromatography column (Thomson Instruments) equilibrated with TBSE. Elution was conducted at a flow rate of 0.75 mL/min and monitored by absorbance at 280 nm. The same amounts of RAE-1 and m152 proteins or gel filtration protein standards [670, 158, 44, 17, and 1.35 kDa (Bio-Rad)] were analyzed separately. Chromatographs were analyzed with 32 Karat (Beckman-Coulter).

Analytical ultracentrifugation experiments were conducted in a Beckman-Coulter (Indianapolis, IN) Optima XLI instrument with An50-Ti rotors, following the protocols previously described (*30*). A series of experiments was conducted with samples at different concentrations ranging from 1.2 to 45 μM and molar ratios of 1:1, 2:1, and 1:2 for the experiments with RAE-1β binding to m152 and at a 1:1 molar ratio for studying the interaction of the other molecules with m152. In brief, for sedimentation velocity (SV) experiments, 400 μL of sample was inserted in 12 mm charcoal-filled Epon centerpieces (100 μL was inserted in 3 mm path length centerpieces for samples at the highest concentrations), sedimented at 50000 rpm and 20 °C, and concentration profiles were recorded using the interference optical system. The data were analyzed by first calculating a diffusion-deconvoluted sedimentation coefficient distribution $c(s)$ with SEDFIT (*31*), followed by integration of the peaks to determine the weight-average s value of the mixture. For RAE-1β, additionally, the amplitude and s value of the reaction boundary and the undisturbed boundary were determined. The resulting isotherm data were globally fitted with models for mass action law and the boundary structure predicted by Gilbert−Jenkins theory, as implemented in SEDPHAT and described in detail elsewhere (*32*). In all analyses, the s values of the separately studied individual components were used as prior knowledge (3.16 and 2.08 S for m152 and RAE-1β, respectively). Error analysis was performed with the Monte Carlo method.

To study the consistency with the results from isothermal titration calorimetry (ITC), a global analysis of the s value isotherms and ITC titration was performed with SEDPHAT, and fractions of nonparticipating molecules of either m152 or RAE-1β were included in the model.

Sedimentation equilibrium (SE) experiments were conducted with 180 μL samples of RAE-1β and m152 at concentrations between 1 and 15 μM at RAE-1β:m152 molar ratios of 1:1, 1:2, and 2:1. Samples were inserted in Epon centerpieces with an optical path length of 12 mm. For detection, the absorbance optics at wavelengths of 280 and 250 nm were used to record concentration profiles sequentially at rotor speeds of 11000 and 17000 rpm, at 4 °C. At each speed, equilibrium was established by assessing the difference in signal of scans at 6 h intervals. Concentration gradients from different loading concentrations, molar ratios, and wavelengths were fitted with theoretical models for sedimentation equilibrium of bimolecular interacting systems forming reversible 1:1 complexes, as described previously (*33*). Statistical errors of the parameter estimates from the SE analysis were determined with F statistics and the projection method. Molar extinction coefficients at 280 nm were determined from amino acid composition using SEDNTERP (courtesy of J. Philo). Separate SE experiments were conducted in the same rotor and results analyzed by global multispeed and multisignal analysis with a single-species model to determine the buoyant molar masses of the individual components (M_b = 10844 Da and M_b = 6855 Da for m152 and RAE-1β, respectively, consistent with the expectation based on amino acid composition). [Note that the buoyant molar mass is $M_b = M(\bar{\nu}\rho)$, where the buoyancy reduces the effective molar mass in sedimentation to approximately $^1/_4$ of the true molar mass]. This also provided the ratios of extinction coefficients at 280, 250, and 230 nm.

m152 (10 μM) was titrated with RAE-1β (100 μM) over 23 injections (4 × 2 μL, 19 × 15 μL) at 25 °C using a VP-ITC microcalorimeter (GE Healthcare). Experimental samples were prepared by size exclusion chromatography (Superdex 75) and diluted to the indicated concentrations with filtered column running buffer [25 mM Tris, 500 mM NaCl, and 10 mM EDTA (pH 7.5)]. Data analysis was performed using the global analysis software SEDPHAT (*34*) applying a 1:1 binary interaction model to obtain values for the apparent enthalpy change and binding constant. Error analysis was performed with the Monte Carlo method. The global analysis of isotherms from SV and ITC was performed with SEDPHAT, assuming the absence of a significant temperature dependence of K_d between 20 and 25 °C. Global analysis of the isothermal titration calorimetry data along with the SV-AUC data of RAE-1β indicates that no more than 8% of the RAE-1β was incompetent monomer.

Molecular Modeling of RAE-1 Isoforms and Mutants. Starting with the 2.85 Å structure of RAE-1β [Protein Data Bank (PDB) entry 1JFM] (*26*) and the Clustal W alignment of the five RAE-1 isoforms shown in Figure 4, we substituted residues of RAE-1β (in the first molecule of the asymmetric unit) with the corresponding residues of RAE-1γ, followed by idealization of geometry in Coot version 0.4.1 (*35*). Similar substitutions were made to generate the RAE-1δ model. To model the PLWY deletion of RAE-1δ, which lies between the β1 and β2 strands, the entire loop consisting of residues Lys12−Tyr22 was deleted and rebuilt initially as poly-Ala, and then individual residues of RAE-1δ were introduced. Electrostatic surface calculations and molecular graphics illustrations were produced with PyMOL (http://www.pymol.org).

RESULTS

m152 Binds to RAE-1 Directly in Vitro. Although several lines of evidence indicate that m152 can downregulate the cell surface expression of RAE-1 in BALB/c mice (*21*), it remains unclear whether this is due to a direct interaction of these molecules. Indeed, previous efforts in several laboratories have failed to demonstrate direct interaction by co-immunoprecipitation or immunoprecipitation and blotting (*20*, *21*, *24*). To examine whether the lumenal MHC-I-like domain of m152 interacts with the lumenal domain of RAE-1, we engineered and purified the ectodomains of these molecules and measured their interactions in a well-defined biochemical environment. As RAE-1 isoforms are expressed at the cell surface as either RAE-1α, -β, or -γ in BALB/c (but not C57BL/6) mice, or RAE-1δ and -ε in C57BL/6 (but not BALB/c) mice (*19*, *20*), we chose RAE-1β, -γ, and -δ as representatives of these two groups. By amino acid sequence (see Figure 4), RAE-1β and -γ may be considered as representative of members of the family that contain the PLWY motif, and δ represents the deletion of the motif. Previous biosynthetic studies have focused on differences between RAE-1γ

and -δ (*24*). The ectodomains of RAE-1β, -γ, and -δ were expressed in bacteria as insoluble inclusion bodies and subsequently solubilized, refolded, and purified. The ectodomain of m152 was expressed as a secreted protein and purified from insect cell supernatants. As shown in panels A and B of Figure 1, both RAE-1 and m152 were purified as monomeric proteins.

To assess the interaction of m152 with different RAE-1 isoforms qualitatively, we analyzed mixtures of these molecules by SEC with columns that resolve differences in the required molecular weight range. SEC, although an inherently qualitative rather than quantitative method, permits rapid assessment of molecular interactions with K_d values in the micromolar range (*36*). RAE-1 and m152 at concentrations of ~50 μM were run on the SEC column either separately or after mixing. A shift of the eluted peak of the mixture to a shorter retention time compared to the peak of RAE-1 or m152 alone revealed the noncovalent direct interaction of the two proteins in solution. As shown in panels C and D of Figure 1, when RAE-1β or -γ was mixed with m152, a peak shift corresponding to the formation of a higher-molecular weight species (i.e., protein complex) was observed. The peak shift was especially apparent with the mixture of RAE-1γ and m152 (Figure 1D), revealing a distinct peak for the complex, suggesting m152 might bind RAE-1γ with higher affinity. In contrast, when RAE-1δ was mixed with m152 (Figure 1E), the peaks superposed essentially with that of m152 alone, suggesting a significantly weaker interaction between RAE-1δ and m152 that cannot be detected by this method. Together, these results suggested a direct interaction between the ectodomains of RAE-1β and -γ and that of m152, prompting further analysis of their interactions (as well as that of RAE-1δ) by other definitive and quantitative means.

m152 Binds to Different RAE-1 Isoforms with 1:1 Stoichiometry but with Differing Affinity. Although SEC experiments suggested that m152 could interact with at least some isoforms of RAE-1, this is not a particularly quantitative technique. Therefore, to characterize quantitatively the interaction between RAE-1 and m152, SV and SE AUC experiments were performed with RAE-1β and m152 under conditions similar to those used in the binding experiment on the SEC column (Figure 2). A range of concentrations covering the expected binding isotherm, as well as different ratios of RAE-1β and m152 proteins, were examined at 20 °C. Figure 2A shows the sedimentation coefficient distribution [$c(s)$] from the SV experiment. In the mixture of RAE-1β and m152, a peak with a higher s value can be discerned that is absent from samples of RAE-1β or m152 alone, indicating the formation of protein complexes (*31*, *37*). The s value of this peak (termed s_{fast}) increases with higher protein concentration, consistent with the presence of a reaction boundary with relatively rapid reversible interactions ($k_{off} > 0.001\ s^{-1}$) (*31*, *32*). The analysis of the isotherms of weight-average (s_w) and reaction boundary (s_{fast}) sedimentation coefficients as a function of protein concentration yielded a best-fit K_d value of 4.1 (3.1−5.1) μM for the RAE-1β−m152 interaction (Figure 2B), which was similar to the K_d derived from global nonlinear least-squares fits of the data acquired from SE experiments conducted at 4 °C [1.7 (1.6−4.9) μM] (Figure 2C) (*30*). Moreover, there was a close fit of all the centrifugation data to a simple 1:1 Langmuir binding model based on a single class of noninteracting binding sites, suggesting RAE-1 binds to m152 at a 1:1 ratio. The SV analysis suggested the presence of 16% unreactive m152 (as noted in Experimental Procedures, analysis of data from the SV experiment independently substantiates that both m152 and

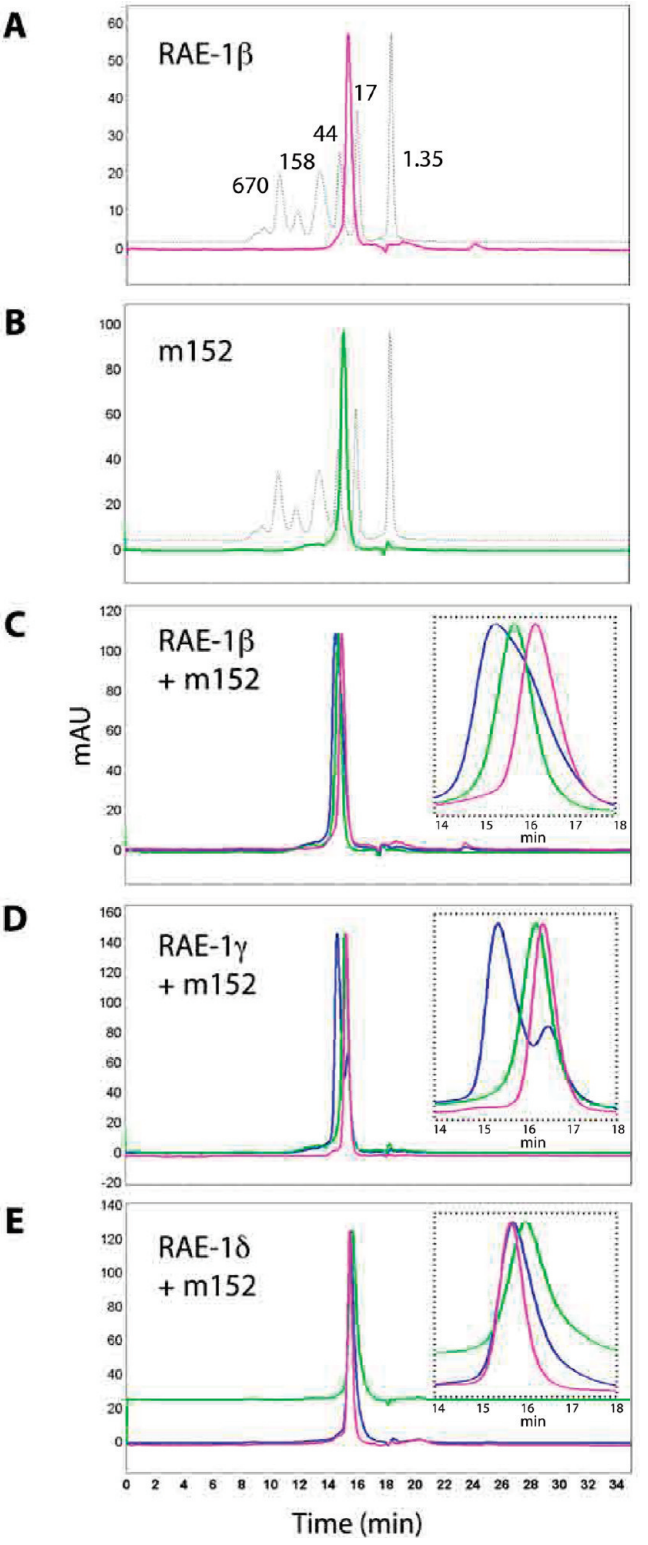

FIGURE 1: m152 binds to RAE-1 directly. (A and B) Purification of RAE-1 and m152. The ectodomains of RAE-1 isoforms and of m152 were expressed and purified as described in Experimental Procedures. Shown here are the chromatographs of RAE-1β (A, pink) and m152 (B, green) overlaid with the protein molecular weight standards (dashed line). (C−E) Binding of m152 to RAE-1β, -γ, and -δ examined by a SEC binding assay. m152 and RAE-1 were mixed in equimolar amounts, incubated for 30 min on ice, and analyzed chromatographically (blue), and the resulting profile was compared to the profile of individual m152 (green) and RAE-1 proteins (pink) alone. Insets show enlargements of the peak regions (flow rate of 0.75 mL/min, so elution volumes may be calculated from the indicated time of elution).

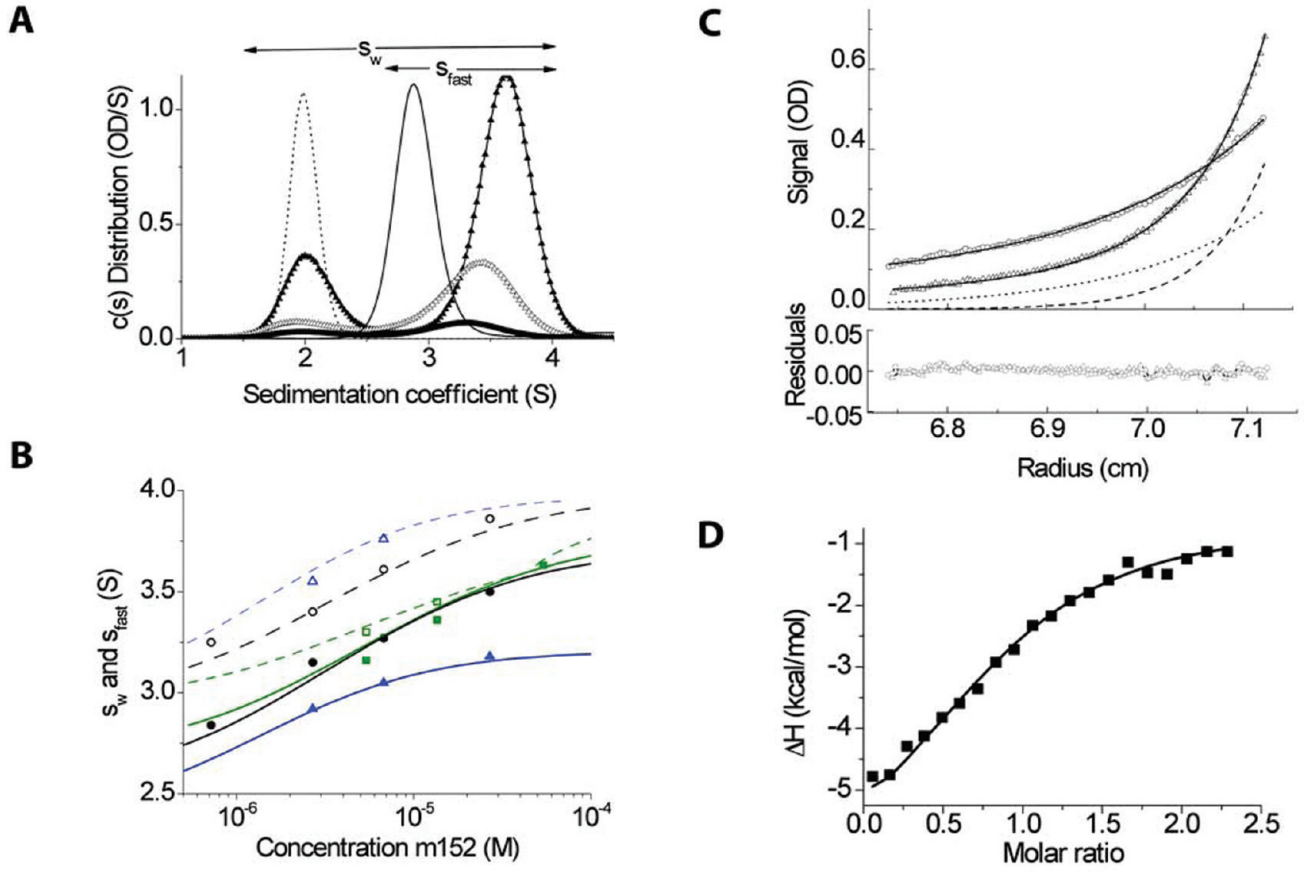

FIGURE 2: Biophysical experiments show m152 binds to RAE-1 at a 1:1 ratio and with a micromolar K_d. (A) Sedimentation coefficient distribution $c(s)$ measured in sedimentation velocity (SV) experiments for 11.3 μM RAE-1 alone (···) and 11.3 μM m152 alone (thin line) and 0.63:1 mixtures of RAE-1 and m152 at 1.2 (thick line), 4.5 (△), and 11.3 μM (▲). Integration of $c(s)$ traces over the range from ~1.5 to ~4.5 S or the range from ~2.5 to ~4.5 S (indicated by horizontal arrows) yields values for the weight-average s value (s_w) or the reaction boundary s value (s_{fast}), respectively. (B) Isotherms of s_w (filled symbols) and s_{fast} (empty symbols) as a function of m152 concentration from dilution series at RAE-1:m152 molar ratios of 1.25:1 (black), 0.63:1 (green), and 2.5:1 (blue). The solid lines shown are from a global fit with a 1:1 binding model that incorporated additional data from the relative amplitude of the reaction boundary, as well as the data from isothermal titration calorimetry (ITC). The best-fit s_w value for the complex was 4.3 S, and the binding constant K_d was 4.1 μM. (C) Equilibrium absorbance profiles at 280 nm of the mixture of 2.9 μM m152 and 10.2 μM RAE-1 sedimenting at 11000 (○) and 17000 rpm (△), their best-fit distribution (solid lines), and the signal predicted for the complex (dotted and dashed lines). These data were taken from a global fit with a 1:1 binding model of 20 equilibrium gradients at different concentrations, rotor speeds, and absorbance wavelengths. (D) Enthalpy isotherm from the titration of 100 μM RAE-1 into 10 μM m152 in ITC (■), based on a single titration series. The solid line shows the best-fit isotherm from a global fit with the SV isotherm data.

RAE-1β were of high purity and were well-folded, globular proteins).

To confirm further the results from both SV and SE experiments and to gain insight into the thermodynamics of the RAE-1β−m152 interaction, isothermal titration calorimetry (ITC) was conducted (Figure 2D) at 25 °C. The results revealed a K_d of 2.1 (1.7−2.7) μM and a 1:1 stoichiometry with 7% (5−9%) unreacted m152 for the interaction between RAE-1β and m152. The thermodynamic parameters of ΔH and $T\Delta S$ were determined to be −6 and 1.44 kcal/mol, respectively, suggesting the interaction is largely enthalpically driven. These results are in good agreement with the AUC measurements, and the results from a global analysis of the s value isotherms from sedimentation velocity and the titration data from ITC indicate the absence of significant temperature dependence of the thermodynamic parameters between 20 and 25 °C.

To examine the differential interaction between RAE-1 isoforms and m152, SV experiments were conducted for RAE-1γ and -δ with m152, and the isotherms of weight-average s values were determined over a range of loading concentrations. Figure 3B shows a comparison of these data for RAE-1β, -γ, and -δ. The K_d derived from the SV data demonstrated a significant difference in the affinity of m152 for different RAE-1 isoforms. RAE-1β and -γ bind to m152 relatively tightly with K_d values of ~3 and ~1 μM, respectively. In contrast, RAE-1δ binds to m152 more weakly, with a K_d of ~30 μM. These results are consistent with the qualitative binding analysis on SEC columns (Figures 1C−E and 3A) and support the view of the differential interaction between m152 and different RAE-1 isoforms. Although apparent differences in the elution time of the three different RAE-1 isoforms can be detected in the SEC profiles of Figure 1C−E, the s values determined from the SV experiments of all six molecules are between 1.92 and 2.05 S, essentially the same.

The PLWY Motif Contributes to the Affinity of RAE-1β for m152. Recent analysis of the comparative function of RAE-1 isoforms noted the deletion of a PLWY motif in RAE-1δ as compared with RAE-1γ (*24*). Since this sequence lies in an exposed loop connecting the β1 and β2 strands (see Figure 6), we hypothesized that it might contribute to the molecular interactions of RAE-1 with m152. To gain insight into the site of interaction and establish the molecular basis for the differential interaction of RAE-1 isoforms with m152, we aligned the amino acid sequences of the five identified RAE-1 isoforms (Figure 4). RAE-1 proteins are more than 90% identical in sequence (*19*).

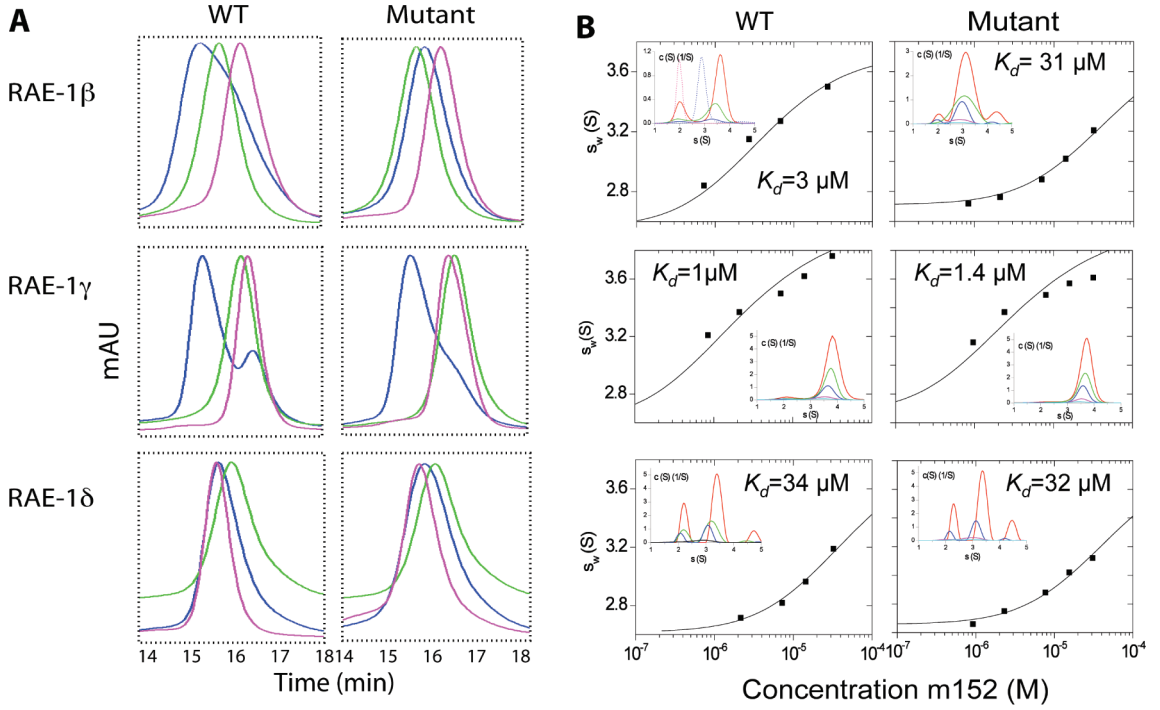

FIGURE 3: PLWY motif that contributes to the binding affinity of RAE-1β for m152. (A) SEC binding assay. The PLWY motif was deleted from RAE-1β and -γ and inserted into RAE-1δ by site-directed mutagenesis. The binding of wild-type and mutant RAE-1 proteins to m152 was examined by SEC as described in Experimental Procedures. The results from wild-type RAE-1 proteins are the same as those shown in Figure 1C−E and shown here for ease of comparison. (B) Sedimentation velocity ultracentrifugation. Isotherms of weight-average sedimentation coefficients s_w (in experimental units) obtained from SV experiments of equimolar mixtures of RAE-1 and m152 (■) and best-fit isotherm with a 1:1 binding model (solid lines) using the predetermined *s* value of RAE-1 and m152, and a complex *s* value fixed to that determined in the extensive characterization of RAE-1β−m152 interaction in Figure 2. The insets show the sedimentation coefficient distributions $c(s)$ underlying the s_w data points, for approximately equimolar loading concentrations of 1 (cyan), 2 (magenta), 7 (blue), 14 (green), and 32 μM (red). Precise concentrations were measured from the interference optical signal and varied slightly.

However, among the several sequence variants, the PLWY motif (amino acids 49−52) is present in RAE-1α, -β, and -γ but is deleted in RAE-1δ and substituted with LPWC in RAE-1ε. The presence or absence of the PLWY motif seems to correlate with RAE-1 function, as RAE-1 proteins are expressed exclusively as two groups (RAE-1α, -β, and -γ or RAE-1δ and -ε) in different mouse strains. We hypothesized that differences in the PLWY motif may contribute to the differential interaction of RAE-1 isoforms with m152 and that the differential interactions might be reflected in the relative control of cell surface expression of the different RAE-1 isoforms under the influence of m152. To test this idea, we constructed PLWY deletion mutants of RAE-1β and -γ, as well as a PLWY addition mutant of RAE-1δ, and expressed, refolded, and purified the ectodomains of these RAE-1 mutants. We then examined the binding interaction between RAE-1 mutants and m152 by SEC and AUC using the same methods we used for wild-type RAE-1 proteins (Figure 3). As shown in Figure 3A, deletion of the PLWY motif from RAE-1β (i.e., the RAE-1β mutant) caused the loss of the more rapidly eluting "mixture" peak detected chromatographically, suggesting weakened binding. However, deletion of PLWY from RAE-1γ or insertion of the motif into RAE-1δ (i.e., RAE-1γ and -δ mutant) had little effect on the apparent binding between RAE-1 and m152. These qualitative SEC results were consistent with the observations made in the AUC experiments (Figure 3B), as deletion of the PLWY motif in RAE-1β led to a 10-fold decrease in affinity (K_d changing from 3.1 to 31 μM), whereas deletion of the motif from RAE-1γ resulted in no significant change in K_d (1 μM as compared with 1.4 μM). Insertion of the motif into RAE-1δ also did not cause any measurable change in the K_d. Thus, these results suggested that the PLWY motif may be involved but is not crucial in mediating the interaction of RAE-1γ or -δ with m152.

m152 Downregulates Surface RAE-1 Expression Differently in Transfected HEK293T Cells. Our in vitro characterization of the RAE-1 and m152 interaction revealed that RAE-1 binds to m152 with a K_d as low as 1 μM and at a 1:1 ratio. The magnitude and stoichiometry of the interaction between RAE-1 and m152 suggest that such direct interaction may contribute to the downregulation of RAE-1 surface expression by m152. To test this idea and evaluate the role of full-length, naturally glycosylated proteins in a cellular system, we transiently transfected human HEK293T cells with either m152 cDNA or a control vector, along with either of the RAE-1γ or -δ cDNAs as well as their corresponding PLWY deletion or PLWY insertion mutants, respectively. A similar experiment has been described previously by Lodoen et al. (*21*). In those experiments, equal amounts of the RAE-1 and m152 cDNA were cotransfected into HEK293T cells. They showed that all the five RAE-1 isoforms were susceptible to downregulation by m152. To explore the relative effects of m152 on the cell surface expression of different RAE-1 isoforms, we transfected HEK293T cells with a constant amount of RAE-1 vector and varied the amount of a cotransfected m152-encoding vector that carried an IRES-GFP (see Figure 5 and Experimental Procedures). Forty-eight hours following transfection, cells were examined by flow cytometry for the expression of GFP as an indication of the transfection efficiency and for surface expression of RAE-1. In Figure 5A, the two-dimensional dot plot of GFP versus RAE-1 for the RAE-1γ wild-type transfection is shown. The level of GFP expression

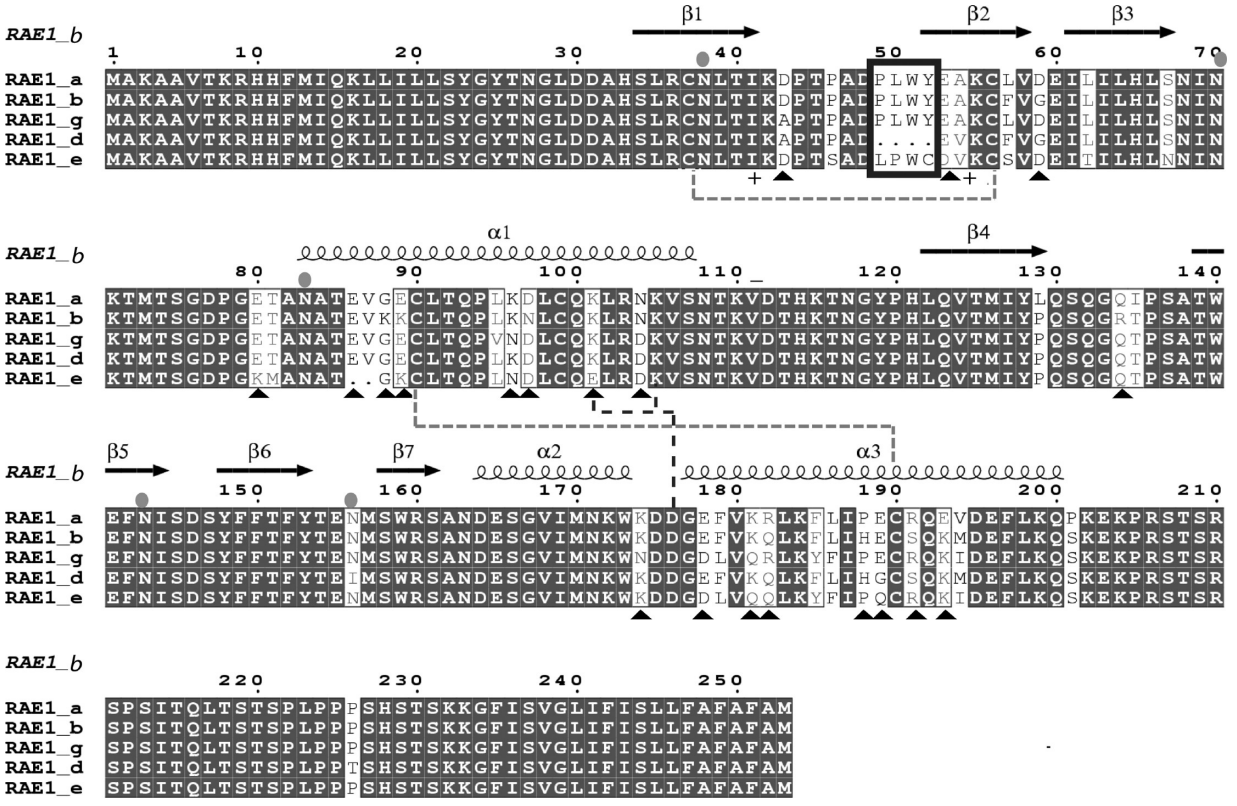

FIGURE 4: RAE-1 isoforms differ in PLWY motif as well as in charged residues. Amino acid sequence alignment of RAE-1 isoforms. The amino acid sequences of the extracellular domain of the five RAE-1 isoforms were aligned using ClustalW (*45*). Secondary structure elements of RAE-1β [PDB entry 1JFM (*26*)] are shown above the alignment. The PLWY motif is boxed in blue. Cysteine residues involved in the formation of disulfide bonds are denoted with gray dashed line. Charged residues involved in the formation of potential salt bridges are denoted with a black dashed line. Differences in charged residues among RAE-1 isoforms are highlighted with black triangles. Predicted N-linked glycosylation sites are denoted with gray circles. The figure was generated with ESPRIPT version 2.2 (*46*).

from IRES-GFP increases steadily with increasing amounts of the IRES-GFP-only vector. RAE-1γ surface expression in the absence of m152 (center column) remains approximately constant, varying from 77% (66.3 + 11%) of total cells for the smallest dose of the empty vector to ~60% (9.83 + 50.6%) with the highest, reflecting some variability apparently due to differences in the total efficiency of transfection. Remarkably, when increasing amounts of the m152-encoding, IRES-GFP vector are included, a progressively smaller proportion of the cells are positive for RAE-1, ranging from 52% (42.5 + 9.74%) of the cells RAE-1 positive at the smallest dose of m152 vector to 16% (8.07+8.39%) at the largest dose. This result is further emphasized if one only considers the GFP^+ cells, where RAE-1 positive cells are 62% (9.74/15.5%) at the smallest dose of m152, 49% (9.41/19.21%) at the intermediate dose, and 21.2% (8.39/38.89%) at the largest dose. Similar two-dimensional analyses were used to generate the histograms for both RAE-1γ and RAE-1δ as well as their respective PLWY deletion and insertion mutants, respectively (Figure 5B). The uninhibited surface expression of RAE-1 is shown by the blue lines, and the m152 downregulated levels are colored green. Thus, it is clear that both RAE-1γ and the RAE-1γ mutant are similarly downregulated by m152 coexpression (Figure 5B, first and second columns). Wild-type RAE-1δ is detectably but less effectively downregulated by m152 than RAE-1γ (Figure 5B, third column) (downregulation of RAE-1δ is not detectable at all at the smallest dose of m152, while for RAE-1γ, there is clearly an effect at that dose). Finally, introduction of the PLWY motif into RAE-1δ, as the RAE-1δ mutant, shows no major difference in m152 responsiveness as compared to that of the wild type. It is crucial to note that "downregulation" of cell surface-expressed RAE-1 isoforms as measured by cell surface immunofluorescent staining formally tells us only that the serological epitopes of RAE-1 are no longer available to the detecting antibody when RAE-1 is coexpressed with m152. The molecular basis for this may be the intracellular interaction of m152 with RAE-1 and subsequent diversion of the normal trafficking of RAE-1 due to the m152 interaction. Alternatively, the m152−RAE-1 complex may go directly to the cell surface at the same rate and with the same steady state level of RAE-1, but with the epitopes of RAE-1 obscured or masked by the binding of m152. However, pulse-chase labeling studies indicated that RAE-1γ, when expressed coordinately with m152, accumulated as lower-molecular weight forms in the ERGIC, consistent with the interpretation that m152−RAE-1γ interaction reduces the level of cell surface expression of the RAE-1γ molecule (*24*).

DISCUSSION

In this study, we hypothesized that the physical interaction between the extracellular domains of the viral protein m152 and the host stress-induced RAE-1 proteins contribute to the regulation of surface expression of RAE-1. Previous efforts to demonstrate the interaction directly by coprecipitation have not been fruitful. Using recombinant RAE-1 isoforms and mutants expressed in *E. coli* and m152 expressed in insect cells, we have demonstrated by several different methods the direct physical interaction of the viral and host-encoded molecules. We have shown that m152 binds RAE-1 directly and at a 1:1 ratio. The binding

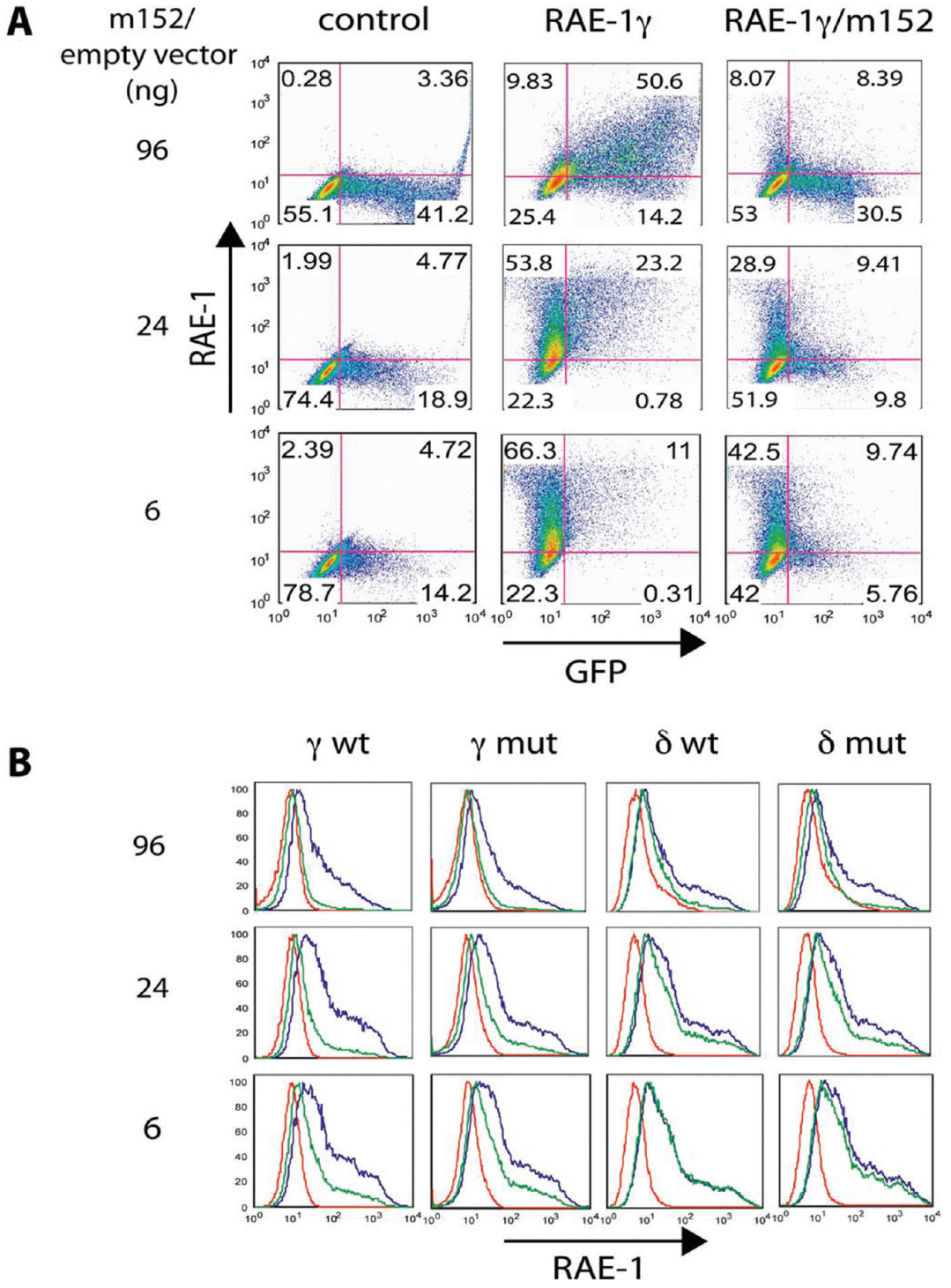

FIGURE 5: m152 differently downregulates surface expression of RAE-1 isoforms. (A) A constant amount of wild type and the PLWY mutant of RAE-1γ or -δ cDNAs were cotransfected into human HEK293T cells along with an empty vector carrying an IRES-GFP (left and middle column) or the corresponding m152-encoding vector (right column) at increasing amounts as indicated. Forty-eight hours after transfection, cells were harvested and stained with either an isotype control Ig (left column) or rat pan anti-RAE-1 mAb (186107, middle and right column) and analyzed for surface RAE-1 expression by flow cytometry. Results are representative of three independent experiments. Shown here is the two-dimensional dot plot of RAE-1γ and m152 cotransfection experiment. (B) Summary of the cotransfection experiments described above in the histogram: red for the isotype control, blue for cotransfected RAE-1 with an empty vector and stained with 186107, and green for cotransfected RAE-1 with m152 and stained with 186107.

affinities differ detectably among RAE-1 isoforms. RAE-1β and -γ, which are expressed on MCMV-susceptible mouse strains such as BALB/c, bind m152 tightly (K_d = 1−3 μM), a level that can be compared to the affinity of the NKG2D−RAE-1 interaction [K_d = 350−730 nM (*28*)]. In contrast, RAE-1δ, which is expressed on MCMV-resistant mouse strains such as C57BL/6, CBA, and C3H, binds m152 weakly (K_d = 34 μM), which is ~50-fold lower than its affinity for NKG2D (K_d = 726 nM). The difference in affinity of RAE-1β or RAE-1γ for m152 as compared with RAE-1δ suggests that the less effective downregulation of RAE-1δ by m152 as reported recently by Arapovic et al. (*24*) may be a result of this lower affinity. It is interesting to

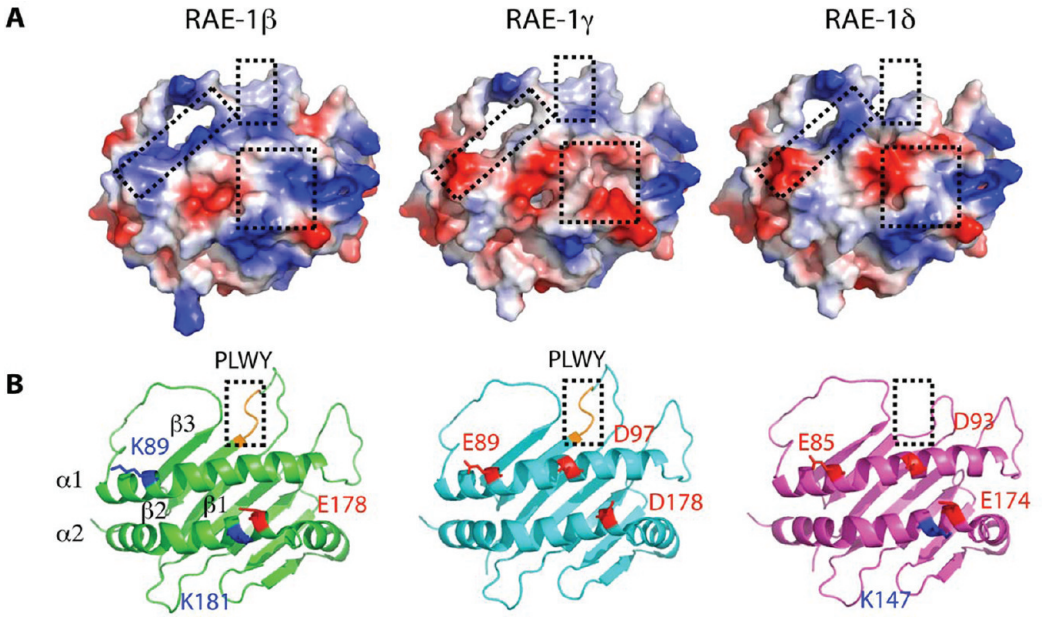

FIGURE 6: RAE-1 isoforms differ in surface electrostatic charge. (A) Models of RAE-1γ and -δ were constructed in Coot based on the crystal structure of RAE-1β [PDB entry 1JFM, chain A (*26*)]. RAE-1β is 92 and 94% identical in amino acid sequence with RAE-1γ and -δ, respectively. Residues in RAE-1β were replaced with the corresponding residues of RAE-1γ and -δ followed by geometry idealization as described in Experimental Procedures. The molecular surfaces are colored by electrostatic potential, with positively charged areas colored blue and negatively charged areas red. (B) Ribbon diagrams of RAE-1β, -γ, and -δ. Positions of some of the polymorphic charged residues are shown as stick representations superposed on the ribbons. For RAE-1β, residues Lys89 (blue), Glu178 (red), and Lys181 (blue) are shown; for RAE-1γ, Glu89 (red), Asp97 (red), and Asp178 (red) are shown, and for RAE-1δ, Glu89 (red), Asp97 (red), Glu178 (red), and Lys181 (blue) are shown (numbering based on the alignment in Figure 4).

note that the SV analysis of the m152−RAE-1β interaction revealed a concentration-dependent increase in s_{fast}, indicative of relatively rapid reversible interaction (Figure 2A). This result may explain the experimental difficulties in detecting m152−RAE-1 interaction by co-immunoprecipitation "pull-down" experiments. Similarly, it was observed that the lumenal domain of m152 is involved in the retention of MHC class I molecules in the ERGIC region in the cells, but without biochemical evidence for their direct interaction (*23*, *38*). This suggests the m152−RAE-1 and m152−MHC-I interactions may share similar intracellular regulatory pathways.

The differing affinities of RAE-1 isoforms for the MCMV m152 immunoevasin suggest a scenario for the ongoing evolution of MCMV immunoevasins. Genetic resistance of different mouse strains to MCMV infection is determined to some degree by loci that control NK activating receptors such as Ly49H (expressed in MCMV-resistant strain C57BL/6) (*39*). In MCMV sensitive strains such as BALB/c, NKG2D, as an ITAM-associated activating receptor, plays an important role in the control of viral titer following infection, and NKG2D ligands, particularly the stress-induced MULT-1, H60, and RAE-1 molecules, serve as the stimulus for NK cell activation. The virus gains a counter-advantage by evolving evasins that antagonize the expression or function of the NKG2D ligands, particularly important in the setting of Ly49H negative mouse strains. These "sensitive" mouse strains may then gain advantage over the virus by the expression of more potent NKG2D ligands such as RAE-1α, -β, and -γ, while the resistant strains, because they have an additional NK activating receptor, Ly49H, have less need for the expression of better NKG2D ligands. In response to the expression of "good" NKG2D ligands, the virus refines the function of molecules to downregulate not only MULT-1 and H60 but also RAE-1α, -β, and -γ, accomplishing this with m152/gp40. The strong direct interaction of the m152 lumenal domain with RAE-1β and -γ as we have measured here results in the effective downregulation of these NKG2D ligands, and the quantitative difference between the interactions of RAE-1β and -γ with m152 as compared with RAE-1δ reflects the greater need for effective control of RAE-1β and -γ (and presumably RAE-1α as well) to counter the NKG2D susceptibility of MCMV-infected cells by NK sensitive strains.

This discussion is based on our knowledge of the genetics and relative resistance of several well-characterized inbred mouse strains, and a more complete analysis would require an extensive understanding of the expression patterns and RAE-1 isoform differences among wild outbred mice. To the best of our knowledge, such data are not yet available. However, the role of the MCMV genes is beginning to be assessed by the analysis of DNA of a number of independent isolates of virus from free-living mice (*40*−*42*) Remarkably, the *m152* gene has been highly conserved, suggesting that its evolutionary advantage is either to encode a protein that interacts with a molecule with conserved structure or to serve multiple functions, such as the dual function of interaction of m152 with both RAE-1 and host MHC-I. Needless to say, these molecules as well as others play a complex cooperative role in the mutual adaptation of virus and host, and our studies of one set of these interactions offer only a hint of the greater complexity. It should be emphasized, however, that the preservation of a gene that contributes to the fitness of the virus may result from a rather small advantage that may elude detection by laboratory evaluation of viral titer resulting from controlled doses and routes of infection.

To understand the molecular mechanisms that determine the differential m152−RAE-1 interaction, we explored whether the PLWY motif, which is present in RAE-1α, -β, and -γ and absent from RAE-1δ and mutated to the LPWC motif in RAE-1ε, may play a role in the m152−RAE-1 interaction. Our results

confirmed that deletion of the PLWY motif in RAE-1β indeed caused a 10-fold decrease in its binding affinity for m152, suggesting that the PLWY motif has a key role in the m152−RAE-1β interaction. However, the binding affinity of RAE-1γ or -δ for m152 was not influenced by the presence or absence of PLWY, indicating that other differences among RAE-1 isoforms contribute to the interaction and to the resulting downregulation of m152. We further found that aside from the PLWY motif, RAE-1 isoforms differ at a number of positions in charged amino acid residues (Figure 4). To gain insight into the possible effects of these amino acid differences, we have examined the surface electrostatic distribution of the RAE-1β X-ray structure and have generated molecular models of RAE-1γ and RAE-1δ as well (Figure 6).

Our first consideration was whether the predicted N-linked glycosylation sites of RAE-1 (Asn38, -70, -83, -143, and -156, all conserved, with the exception of Asn156 which is absent from RAE-1δ) might impinge on the m152 interaction. All of these are distant from the NKG2D−RAE-1 interface (*26*) and are located either beneath the platform domain (Asn38 and -143) or at various peripheral positions (Asn83 at the N-terminus of helix α1 and Asn70 and -156 in loops connecting β-strands). Thus, we focused on the "top" of the RAE-1 molecule, which serves as the NKG2D binding interface (*26*).

Looking at a top view of the RAE-1β structure in comparison with the models, we find there are three major regions that seem to be influenced by the substitutions that distinguish the three isoforms. The first and most obvious region is that in which the PLWY motif is present in RAE-1β and -γ and the PLWY motif is deleted in RAE-1δ. This region flanks helix α1, focused on the loop connecting strands β1 and β2. The second major area involves the third β-strand of domain α1 as well as the left-hand side of helix α1 (see the left box in Figure 6A and highlighted residues of helix α1 in Figure 6B). This region is basic in RAE-1β, acidic in RAE-1γ, and partly acidic and partly basic in RAE-1δ. The third region spans the right-hand side of both the α1 and α2 helices, is basic in RAE-1β and acidic in RAE-1γ, and has subregions of both acidic and basic character in RAE-1δ. A more detailed understanding clarifying the complexities of the interaction of m152 with the various RAE-1 isoforms must await the determination of the structure of a complex of RAE-1 with m152. Whether the downregulation of host MHC-I molecules by m152 expression is due to a direct interaction of m152 with MHC-I and whether such a direct interaction is mediated by a surface of MHC-I structurally homologous to that of RAE-1 are questions that demand further detailed investigation.

MCMV infection provides a valid model system not only for understanding available mechanisms for NK and T cell-mediated immunity to infection and virus resistance to host immunity but also for gaining insight into the ongoing coevolution of virus and host. Our studies of the relative differences in the interaction of the viral immunoevasin m152 with host NKG2D ligands provide a glimpse of the ongoing adaptations of virus and host. The recently identified H60 isoforms (H60a, -b, and -c) exhibit some features similar to those of the RAE-1 isoforms (*43*, *44*). The relative interactions of m155 for the different H60 isoforms have yet to be addressed. Thus, differential expression and regulation of host ligands for NKG2D, as influenced by the virus, seem to be common features of the ongoing interplay and evolution of host response and viral immunoevasion. The likelihood that mouse and human viruses may share similar immune evasion strategies raises the prospect for identifying targets for novel antiviral therapeutics based on disrupting the interaction between immunoevasins and their specific ligands in the host.

ACKNOWLEDGMENT

We thank Andrea Balbo for help with the ultracentrifugation experiments and Dr. John Coligan for critical comments on the manuscript.

REFERENCES

1. Lenac, T., Arapovic, J., Traven, L., Krmpotic, A., and Jonjic, S. (2008) Murine cytomegalovirus regulation of NKG2D ligands. *Med. Microbiol. Immunol. 197*, 159–166.
2. Miller-Kittrell, M., and Sparer, T. E. (2009) Feeling manipulated: Cytomegalovirus immune manipulation. *Virol. J. 6*, 4.
3. Powers, C., DeFilippis, V., Malouli, D., and Fruh, K. (2008) Cytomegalovirus immune evasion. *Curr. Top. Microbiol. Immunol. 325*, 333–359.
4. French, A. R., and Yokoyama, W. M. (2003) Natural killer cells and viral infections. *Curr. Opin. Immunol. 15*, 45–51.
5. Doom, C. M., and Hill, A. B. (2008) MHC class I immune evasion in MCMV infection. *Med. Microbiol. Immunol. 197*, 191–204.
6. Wagner, M., Gutermann, A., Podlech, J., Reddehase, M. J., and Koszinowski, U. H. (2002) Major histocompatibility complex class I allele-specific cooperative and competitive interactions between immune evasion proteins of cytomegalovirus. *J. Exp. Med. 196*, 805–816.
7. Tortorella, D., Gewurz, B. E., Furman, M. H., Schust, D. J., and Ploegh, H. L. (2000) Viral subversion of the immune system. *Annu. Rev. Immunol. 18*, 861–926.
8. Raulet, D. H. (2003) Roles of the NKG2D immunoreceptor and its ligands. *Nat. Rev. Immunol. 3*, 781–790.
9. Gonzalez, S., Groh, V., and Spies, T. (2006) Immunobiology of human NKG2D and its ligands. *Curr. Top. Microbiol. Immunol. 298*, 121–138.
10. Lanier, L. L. (2001) On guard: Activating NK cell receptors. *Nat. Immunol. 2*, 23–27.
11. Bauer, S., Groh, V., Wu, J., Steinle, A., Phillips, J. H., Lanier, L. L., and Spies, T. (1999) Activation of NK cells and T cells by NKG2D, a receptor for stress-inducible MICA. *Science 285*, 727–729.
12. Gasser, S., Orsulic, S., Brown, E. J., and Raulet, D. H. (2005) The DNA damage pathway regulates innate immune system ligands of the NKG2D receptor. *Nature 436*, 1186–1190.
13. Strid, J., Roberts, S. J., Filler, R. B., Lewis, J. M., Kwong, B. Y., Schpero, W., Kaplan, D. H., Hayday, A. C., and Girardi, M. (2008) Acute upregulation of an NKG2D ligand promotes rapid reorganization of a local immune compartment with pleiotropic effects on carcinogenesis. *Nat. Immunol. 9*, 146–154.
14. Arapovic, J., Lenac Rovis, T., Reddy, A. B., Krmpotic, A., and Jonjic, S. (2009) Promiscuity of MCMV immunoevasin of NKG2D: m138/fcr-1 down-modulates RAE-1 ε in addition to MULT-1 and H60. *Mol. Immunol. 47*, 114–122.
15. Lenac, T., Budt, M., Arapovic, J., Hasan, M., Zimmermann, A., Simic, H., Krmpotic, A., Messerle, M., Ruzsics, Z., Koszinowski, U. H., Hengel, H., and Jonjic, S. (2006) The herpesviral Fc receptor fcr-1 down-regulates the NKG2D ligands MULT-1 and H60. *J. Exp. Med. 203*, 1843–1850.
16. Gutermann, A., Bubeck, A., Wagner, M., Reusch, U., Menard, C., and Koszinowski, U. H. (2002) Strategies for the identification and analysis of viral immune-evasive genes: Cytomegalovirus as an example. *Curr. Top. Microbiol. Immunol. 269*, 1–22.
17. Krmpotic, A., Busch, D. H., Bubic, I., Gebhardt, F., Hengel, H., Hasan, M., Scalzo, A. A., Koszinowski, U. H., and Jonjic, S. (2002) MCMV glycoprotein gp40 confers virus resistance to CD8+ T cells and NK cells in vivo. *Nat. Immunol. 3*, 529–535.
18. Yewdell, J. W., and Hill, A. B. (2002) Viral interference with antigen presentation. *Nat. Immunol. 3*, 1019–1025.
19. Cerwenka, A., Bakker, A. B., McClanahan, T., Wagner, J., Wu, J., Phillips, J. H., and Lanier, L. L. (2000) Retinoic acid early inducible genes define a ligand family for the activating NKG2D receptor in mice. *Immunity 12*, 721–727.
20. Diefenbach, A., Jamieson, A. M., Liu, S. D., Shastri, N., and Raulet, D. H. (2000) Ligands for the murine NKG2D receptor: Expression by tumor cells and activation of NK cells and macrophages. *Nat. Immunol. 1*, 119–126.
21. Lodoen, M., Ogasawara, K., Hamerman, J. A., Arase, H., Houchins, J. P., Mocarski, E. S., and Lanier, L. L. (2003) NKG2D-mediated natural killer cell protection against cytomegalovirus is impaired by

viral gp40 modulation of retinoic acid early inducible 1 gene molecules. *J. Exp. Med. 197*, 1245–1253.
22. Pinto, A. K., Jamieson, A. M., Raulet, D. H., and Hill, A. B. (2007) The role of NKG2D signaling in inhibition of cytotoxic T-lymphocyte lysis by the murine cytomegalovirus immunoevasin m152/gp40. *J. Virol. 81*, 12564–12571.
23. Ziegler, H., Muranyi, W., Burgert, H. G., Kremmer, E., and Koszinowski, U. H. (2000) The luminal part of the murine cytomegalovirus glycoprotein gp40 catalyzes the retention of MHC class I molecules. *EMBO J. 19*, 870–881.
24. Arapovic, J., Lenac, T., Antulov, R., Polic, B., Ruzsics, Z., Carayannopoulos, L. N., Koszinowski, U. H., Krmpotic, A., and Jonjic, S. (2009) Differential susceptibility of RAE-1 isoforms to mouse cytomegalovirus. *J. Virol. 83*, 8198–8207.
25. Mans, J., Natarajan, K., Balbo, A., Schuck, P., Eikel, D., Hess, S., Robinson, H., Simic, H., Jonjic, S., Tiemessen, C. T., and Margulies, D. H. (2007) Cellular expression and crystal structure of the murine cytomegalovirus major histocompatibility complex class I-like glycoprotein, m153. *J. Biol. Chem. 282*, 35247–35258.
26. Li, P., McDermott, G., and Strong, R. K. (2002) Crystal structures of RAE-1β and its complex with the activating immunoreceptor NKG2D. *Immunity 16*, 77–86.
27. Natarajan, K., Hicks, A., Mans, J., Robinson, H., Guan, R., Mariuzza, R. A., and Margulies, D. H. (2006) Crystal structure of the murine cytomegalovirus MHC-I homolog m144. *J. Mol. Biol. 358*, 157–171.
28. O'Callaghan, C. A., Cerwenka, A., Willcox, B. E., Lanier, L. L., and Bjorkman, P. J. (2001) Molecular competition for NKG2D: H60 and RAE1 compete unequally for NKG2D with dominance of H60. *Immunity 15*, 201–211.
29. Brown, P. H., Balbo, A., and Schuck, P. (2008) A Bayesian approach for quantifying trace amounts of antibody aggregates by sedimentation velocity analytical ultracentrifugation. *AAPS J. 10*, 481–493.
30. Balbo, A., Brown, P. H., Braswell, E. H., and Schuck, P. (2007) Measuring protein-protein interactions by equilibrium sedimentation. Current Protocols in Immunology, Chapter 18, Unit 18, p 18, Wiley, New York.
31. Schuck, P. (2000) Size-distribution analysis of macromolecules by sedimentation velocity ultracentrifugation and Lamm equation modeling. *Biophys. J. 78*, 1606–1619.
32. Dam, J., and Schuck, P. (2005) Sedimentation velocity analysis of heterogeneous protein-protein interactions: Sedimentation coefficient distributions c(s) and asymptotic boundary profiles from Gilbert-Jenkins theory. *Biophys. J. 89*, 651–666.
33. Vistica, J., Dam, J., Balbo, A., Yikilmaz, E., Mariuzza, R. A., Rouault, T. A., and Schuck, P. (2004) Sedimentation equilibrium analysis of protein interactions with global implicit mass conservation constraints and systematic noise decomposition. *Anal. Biochem. 326*, 234–256.
34. Houtman, J. C., Brown, P. H., Bowden, B., Yamaguchi, H., Appella, E., Samelson, L. E., and Schuck, P. (2007) Studying multisite binary and ternary protein interactions by global analysis of isothermal titration calorimetry data in SEDPHAT: Application to adaptor protein complexes in cell signaling. *Protein Sci. 16*, 30–42.
35. Emsley, P., and Cowtan, K. (2004) Coot: Model-building tools for molecular graphics. *Acta Crystallogr. D60*, 2126–2132.
36. Mayer, C. L., Snyder, W. K., Swietlicka, M. A., Vanschoiack, A. D., Austin, C. R., and McFarland, B. J. (2009) Size-exclusion chromatography can identify faster-associating protein complexes and evaluate design strategies. *BMC Res. Notes 2*, 135.
37. Brown, P. H., Balbo, A., and Schuck, P. (2008) Characterizing protein-protein interactions by sedimentation velocity analytical ultracentrifugation, Current Protocols in Immunology, Chapter 18, Unit 18, p 15, Wiley, New York.
38. Ziegler, H., Thale, R., Lucin, P., Muranyi, W., Flohr, T., Hengel, H., Farrell, H., Rawlinson, W., and Koszinowski, U. H. (1997) A mouse cytomegalovirus glycoprotein retains MHC class I complexes in the ERGIC/cis-Golgi compartments. *Immunity 6*, 57–66.
39. Scalzo, A. A., and Yokoyama, W. M. (2008) Cmv1 and natural killer cell responses to murine cytomegalovirus infection. *Curr. Top. Microbiol. Immunol. 321*, 101–122.
40. Smith, L. M., McWhorter, A. R., Masters, L. L., Shellam, G. R., and Redwood, A. J. (2008) Laboratory strains of murine cytomegalovirus are genetically similar to but phenotypically distinct from wild strains of virus. *J. Virol. 82*, 6689–6696.
41. Smith, L. M., Shellam, G. R., and Redwood, A. J. (2006) Genes of murine cytomegalovirus exist as a number of distinct genotypes. *Virology 352*, 450–465.
42. Mans, J., Zhi, L., Revilleza, M. J., Smith, L., Redwood, A., Natarajan, K., and Margulies, D. H. (2009) Structure and function of murine cytomegalovirus MHC-I-like molecules: How the virus turned the host defense to its advantage. *Immunol. Res. 43*, 264–279.
43. Takada, A., Yoshida, S., Kajikawa, M., Miyatake, Y., Tomaru, U., Sakai, M., Chiba, H., Maenaka, K., Kohda, D., Fugo, K., and Kasahara, M. (2008) Two novel NKG2D ligands of the mouse H60 family with differential expression patterns and binding affinities to NKG2D. *J. Immunol. 180*, 1678–1685.
44. Whang, M. I., Guerra, N., and Raulet, D. H. (2009) Costimulation of dendritic epidermal gammadelta T cells by a new NKG2D ligand expressed specifically in the skin. *J. Immunol. 182*, 4557–4564.
45. Chenna, R., Sugawara, H., Koike, T., Lopez, R., Gibson, T. J., Higgins, D. G., and Thompson, J. D. (2003) Multiple sequence alignment with the Clustal series of programs. *Nucleic Acids Res. 31*, 3497–3500.
46. Gouet, P., Courcelle, E., Stuart, D. I., and Metoz, F. (1999) ESPript: Analysis of multiple sequence alignments in PostScript. *Bioinformatics 15*, 305–308.